SINTEF
PROCEEDINGS 6

14th International Conference on CFD in
Oil & Gas, Metallurgical and Process Industries
SINTEF, Trondheim, Norway, October 12–14, 2020

Proceedings from the 14th International Conference on CFD in Oil & Gas, Metallurgical and Process Industries

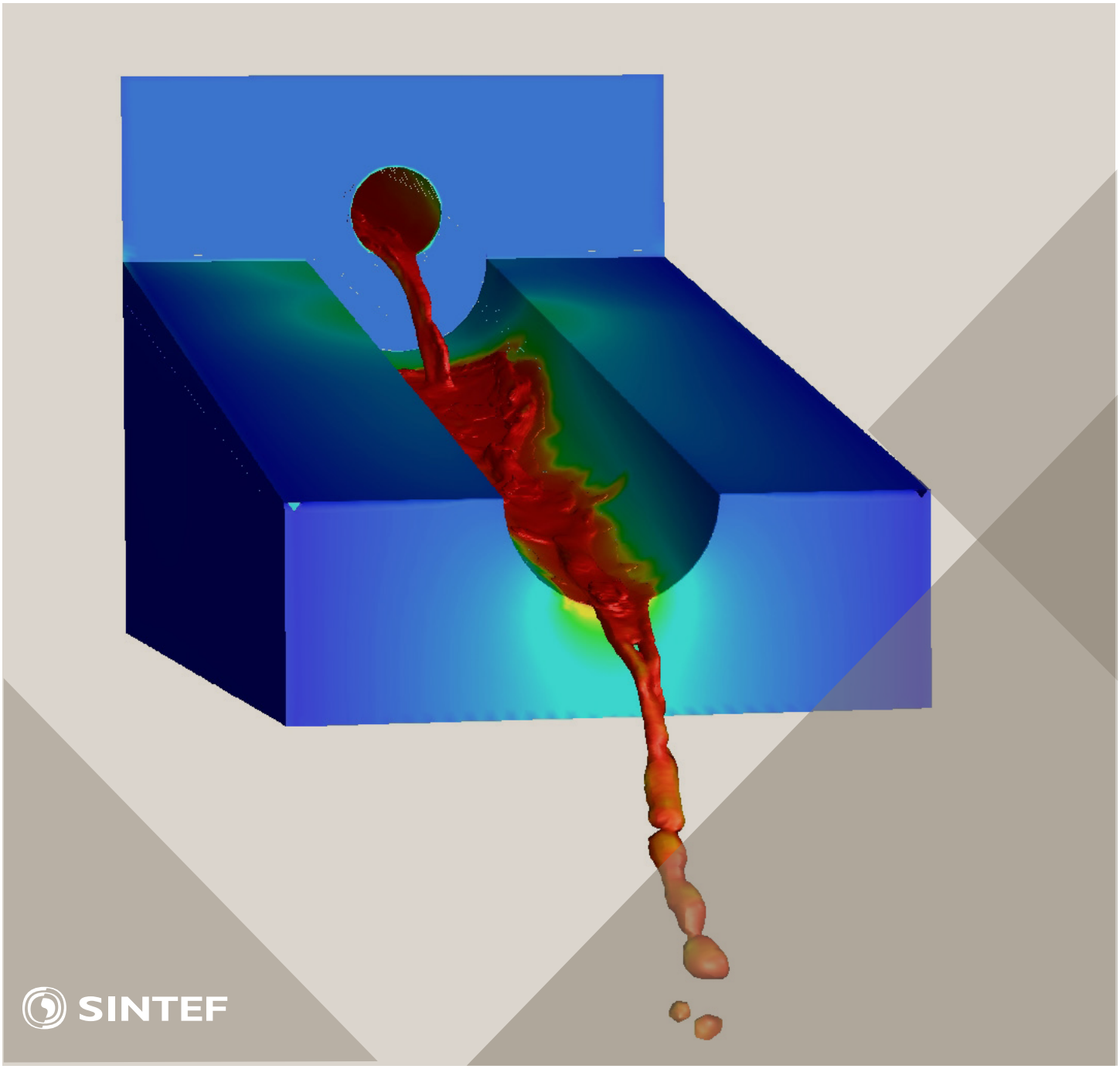

SINTEF Proceedings

Editors:
Jan Erik Olsen, Jan Hendrik Cloete and Stein Tore Johansen

Proceedings from the 14th International Conference on CFD in Oil & Gas, Metallurgical and Process Industries

SINTEF, Trondheim, Norway
October 12–14, 2020

SINTEF Academic Press

SINTEF Proceedings 6
Editors: Jan Erik Olsen, Jan Hendrik Cloete and Stein Tore Johansen

Proceedings from the 14th International Conference on CFD in Oil & Gas, Metallurgical and Process Industries, SINTEF, Trondheim, Norway, October 12–14, 2020

Keywords:
CFD, fluid dynamics, modelling

Cover illustration: Tapping of metal by Jan Erik Olsen

ISSN 2387-4295 (online)
ISBN 978-82-536-1684-1 (pdf)

SINTEF Academic Press
Address: Børrestuveien 3
PO Box 124 Blindern
N-0314 OSLO
Tel: +47 40 00 51 00

www.sintef.no/community
www.sintefbok.no

14th International Conference on CFD in Oil & Gas, Metallurgical and Process Industries
SINTEF, Trondheim, NORWAY
October 12-14, 2020

COMBINING AN IMPLICIT SOLUTION WITH AN EXPLICIT CORRECTOR STEP FOR THE SOLUTION OF THE CONTINUITY EQUATIONS IN A TWO-FLUID SOLVER

Eva-Maria WARTHA[1*], **Markus BÖSENHOFER**[12], **Michael HARASEK**[1]

[1]Technische Universität Wien - Institute of Chemical Environmental and Bioscience Engineering, 1060 Vienna, Austria

[2]K1-MET GmbH, Area 4 - Simulation and Analyses, Linz, Austria

* E-mail: eva-maria.wartha@tuwien.ac.at

ABSTRACT

To model two-phase flows in industrial applications, for example the raceway zone in a blast furnace, an Eulerian two-fluid model is usually the method of choice. It has proven to predict the behavior of gas-solid flows well and has a justifiable computational demand. Although, it is already widely used, there are still some deficiencies which arise from the averaged equations. Especially the continuity equation needs some special care compared to single phase flows. The consistency and boundedness need to be ensured, which is not straightforward. One widely used approach to target this problem is to use the relative velocities in the continuity equation. A drawback is, that this modified equation is non-linear in the phase fraction and therefore needs to be solved iteratively if solved implicitly. We propose to solve the discretized equation by combining an implicit solution step with (an) explicit corrector step(s). This new approach was implemented in the open source software OpenFOAM® and compared with the standard implementation. The new algorithm gives good prediction results for several test cases and this implicit approach could lead to larger time steps through better stability of the solution procedure.

Keywords: Two-Fluid Flow, Euler-Euler Approach, Raceway Simulation .

NOMENCLATURE

Greek Symbols

α	Phase fraction, $[-]$
η	Constant = 2 $[-]$
κ	Solid conductivity $[kg/ms]$
λ	Blending coefficient $[-]$
ξ	Coupling term, $[s^{-1}]$
ρ	Density, $[kg/m^3]$
τ	Stress tensor, $[kg/ms^2]$
ϕ	Angle of internal friction $[\circ]$
φ	Velocity, $[m/s]$

Latin Symbols

p	Pressure, $[Pa]$.
t	Time, $[s]$
A	Diagonal contributions
F	Flux $[m/s]$
Fr	Constant = 0.05 $[-]$
K	Drag coefficient $[kg/m^3 s]$
P	Constant = 5 $[-]$
S	Source term
V	Cell volume$[-]$
$(I_{2D})^{-1/2}$	2nd-order deviatoric shear stress tensor
$\mathbf{g}$	Gravitational acceleration $[m/s^2]$
$\mathbf{S}$	Surface normal vector $[-]$
$\mathbf{U}$	Velocity, $[m/s]$

Sub/superscripts

e	Explicit
f	Face value
g	Gas
i	Implicit
n	Time step
p	Center value
r	Relative value
s	Solid
C	Convective
H	High order
L	Low order
$fric$	Frictional
$ktgf$	Kinetic theory of granular flows
min	Minimum for frictional effects
max	Maximum (packing) limit
$*$	Quantity enlarged with decoupling terms

INTRODUCTION

Industrial processes often incorporate two- or multi-phase flows, for example: fluidized beds for pyrolysis (Papadikis *et al.*, 2008) or the blast furnace for pig iron production (Abhale *et al.*, 2020). The simulation of such processes using computational fluid dynamics (CFD) helps to understand and improve them. To accurately and efficiently predict the phenomena dominating the operation, well calibrated models and numerical procedures are essential.

In general, the solid phase in a two-phase flow could be described by using Lagrangian or Eulerian models. The Lagrangian models offer more detail, since they are able to resolve particle interactions on a per particle basis (van der Hoef *et al.*, 2008; Agrawal *et al.*, 2001). Although, computer power is and has been increasing, the computational demand is still limiting. Therefore, this approach is usually only applied to small scales or low solid concentrations. For the many two-phase flows in industry, which incorporate dense solid flows, the Eulerian models are the way to go, (van der Hoef *et al.*, 2008). Here, both (gas and solid) phases are treated as interpenetrating continua. Particle interactions

can not be resolved using those models but the models have proven to correctly predict phenomena in two-phase flows.
Compared to single-phase flows, the coupled equations are more difficult to solve and need special treatment, (Passalacqua and Fox, 2011; Weller, 2005). To further speed-up simulations the community is constantly trying to improve the algorithms to solve the equations. In this paper we suggest an alternative algorithm for the solution of the continuity equation in two-phase flows.
The algorithmic approach is described in the following section. The new approach was implemented in OpenFOAM® and tested on several test cases. The results are presented and provide promising results for the application of the new algorithm.

THEORY

Two-Fluid solvers are widely used for dense gas-solid systems. They treat both the phases as interpenetrating continua and use the Navier-Stokes equations for their description. Compared to a single-fluid system, the phase fraction is added to the descriptive equations. The phase-averaged equations for the solid phase are given in the following. Eq. 1 shows the continuity equation and Eq. 2 the momentum equation, where α_s is the solid phase volume fraction, $\mathbf{U}_s$ the solid velocity and $\mathbf{U}_g$ the gas velocity, ρ_s the solid density, τ_s the solid stress tensor, p the pressure, p_s the solid pressure, $\mathbf{g}$ the gravitational acceleration and K_{sg} the drag interaction coefficient. The solid pressure p_s is modeled based on the Kinetic Theory of Granular Flows, which is shortly described in a following section.

$$\frac{\partial}{\partial t}\left(\alpha_s \rho_s\right) + \nabla \cdot \left(\alpha_s \rho_s \mathbf{U}_s\right) = 0 \tag{1}$$

$$\begin{aligned}\frac{\partial}{\partial t}\left(\alpha_s \rho_s \mathbf{U}_s\right) + \nabla \cdot \left(\alpha_s \rho_s \mathbf{U}_s \mathbf{U}_s\right) = \nabla \cdot \left(\alpha_s \tau_s\right) \\ -\alpha_s \nabla p - \nabla p_s + \alpha_s \rho_s \mathbf{g} + K_{sg}\left(\mathbf{U}_g - \mathbf{U}_s\right)\end{aligned} \tag{2}$$

The equations for the gas phase are formulated similarly by using the quantities of the gas phase (gas volume fractionα_g, gas density ρ_g and gas stress tensor τ_g):

$$\frac{\partial}{\partial t}\left(\alpha_g \rho_g\right) + \nabla \cdot \left(\alpha_g \rho_g \mathbf{U}_g\right) = 0 \tag{3}$$

$$\begin{aligned}\frac{\partial}{\partial t}\left(\alpha_g \rho_g \mathbf{U}_g\right) + \nabla \cdot \left(\alpha_g \rho_g \mathbf{U}_g \mathbf{U}_g\right) = \nabla \cdot \left(\alpha_g \tau_g\right) \\ -\alpha_g \nabla p + \alpha_g \rho_g \mathbf{g} + K_{sg}\left(\mathbf{U}_s - \mathbf{U}_g\right)\end{aligned} \tag{4}$$

The two phases are coupled through the momentum exchange terms. In Eq. 2 and Eq. 4 only the drag term is considered ($K_{sg}\left(\mathbf{U}_g - \mathbf{U}_s\right)$). Furthermore, the following condition links the phases:

$$\sum \alpha_i = \alpha_s + \alpha_g = 1 \tag{5}$$

With the phase-averaged equations, some problems arise in the solution procedure, because the conservativeness of the solution and the boundedness of the phase volume fraction need to be ensured. Rusche (2002) and Oliveira and Issa (2003) recap different approaches of the discretization of the continuity equation. Here (and in OpenFOAM®) we use an approach presented by (Weller, 2005) and (Passalacqua and Fox, 2011) where the equation is reformulated in the following way:

$$\frac{\partial}{\partial t}\left(\alpha_s\right) + \nabla \cdot \left(\alpha_s \mathbf{U}\right) + \nabla \cdot \left(\alpha_g \alpha_s \mathbf{U}_r\right) = 0 \tag{6}$$

using the average phase velocity $\mathbf{U}$

$$\mathbf{U} = \alpha_s \mathbf{U}_s + \alpha_g \mathbf{U}_g \tag{7}$$

and the relative phase velocity $\mathbf{U}_r$

$$\mathbf{U}_r = \mathbf{U}_s - \mathbf{U}_g \tag{8}$$

The derivation of the coupling terms and the phase pressure yields the modified phase continuity equation, derived by (Passalacqua and Fox, 2011):

$$\begin{aligned}\frac{\partial \alpha_s}{\partial t} + \nabla \cdot \left(\alpha_{s,f} \varphi^*\right) + \nabla \cdot \left(\alpha_g \alpha_s \varphi^*_{r,s}\right) \\ -\nabla \cdot \left[\alpha_{s,f} \xi_{s,f} \left(\frac{1}{\rho_s} \frac{\partial p_s}{\partial \alpha_s}\right)|_f \left|\mathbf{S}\right| \nabla^{\perp} \alpha_s\right] = 0\end{aligned} \tag{9}$$

Where $\mathbf{S}$ is the surface normal vector and the averaged flux (φ) (Eq. 11) and the relative flux ($\varphi_{r,s}$) (Eq. 13) are used. The fluxes (φ^* and $\varphi^*_{r,s}$) are modified by a term resulting from the decoupling of the momentum equations:

$$\varphi^* = \varphi + \alpha_{s,f} \xi_{s,f} \left(\frac{1}{\rho_s} \frac{\partial p_s}{\partial \alpha_s}\right)_f \left|\mathbf{S}\right| \nabla^{\perp} \alpha_s \tag{10}$$

$$\varphi = \alpha_s \varphi_s + \alpha_g \varphi_g \tag{11}$$

$$\varphi^*_{r,s} = \varphi_{r,s} + \xi_{s,f} \left(\frac{1}{\rho_s} \frac{\partial p_s}{\partial \alpha_s}\right)_f \left|\mathbf{S}\right| \nabla^{\perp} \alpha_s \tag{12}$$

$$\varphi_{r,s} = \varphi_s - \varphi_g \tag{13}$$

$$\xi_{s,f} = \frac{1}{A_s + \frac{K_{sg}}{\rho_s}} \tag{14}$$

The partially implicit algorithm (explained by (Weller, 2005) and (Venier *et al.*, 2018)) is used for the decoupling. The term $\xi_{s,f}$ results from this decoupling of the momentum equations - in Eq. 14 only the drag term (K_{sg}) is mentioned, but also the implicit part of the virtual mass force term can be added to $\xi_{s,f}$. A_s is the coefficient matrix arising from the discretisation of the momentum equation.
Boundedness can only be ensured, if a fully implicit solution algorithm is chosen (Rusche, 2002; Passalacqua and Fox, 2011), but the non-linearity in α (Eq. 9) requires subiterations when using an implicit approach.
An upwind differencing scheme can also ensure the boundedness of the solution of Eq. 9. A drawback from the upwind schemes is numerical diffusion and consequently unsatisfying results. Therefore, an algorithm, called MULES (Multidimensional Universal Limiter with Explicit Solution) for blending high-order and upwind solution has been introduced in OpenFOAM® . The MULES algorithm is described in the next section.
Since this MULES algorithm requires quite small time stepping, ≤ 0.25 (Wardle and Weller, 2013), we wanted to suggest a new algorithm to possibly combine the benefits of a fully implicit and the MULES algorithm. This suggested and newly implemented algorithm, named ICMULES, is introduced afterwards and tested on several benchmark cases.

MULES Algorithm

MULES is the abbreviation for "Multidimensional Universal Limiter with Explicit Solution" and is an iterative algorithm to solve hyperbolic equations (Tacconi, 2018). The method explicitly integrates in time and uses a blending of first-order upwind and high-order schemes for the calculation of the fluxes. This ensures the boundedness while keeping the influence of numerical diffusion low.

In the OpenFOAM® Code the *MULES:explicitSolve* function is used to partly solve the modified continuity Eq. 9. The function solves Eq. 9 without the consideration of the last term, see Eq. 15. F^n_{Cf} denotes the convective fluxes, which correspond to the second and third term in Eq. 9. The fluxes are calculated with consideration of the lower ($\alpha = 0$) and upper (α_{max}) limits of the phase fraction. S_i and S_e represent the source terms of the continuity equation arising from f.ex. phase change or compression.

$$\frac{\alpha^{n+1}_{sp} - \alpha^n_p}{\Delta t} V_p + \sum_f F^n_{Cf} = \alpha^{n+1}_{sp} S_i + S_e \qquad (15)$$

The fluxes are blended by fluxes calculated with a low order discretisation scheme F^L_C and fluxes calculated with a high order discretisation scheme F^H_C. The low order and an antidiffusive flux A are summed up, see Eq. 17. The antidiffusive flux is calculated as:

$$A = \left(F^H_C - F^L_C\right) \qquad (16)$$

A limiter function λ, based on the limits of α_s and the neighboring cell values is computed, which determines the degree of blending.

$$\frac{\alpha^{n+1}_{sp} - \alpha^n_{sp}}{\Delta t} V_p + \sum_f F^{n,L}_{Cf} + \sum_f \lambda_f A = \alpha^{n+1}_{sp} S_i + S_e \qquad (17)$$

More details on the computation of the limiter λ are given in (Tacconi, 2018).

ICMULES Algorithm

The suggested new algorithm combines an implicit solution step with a corrector step using MULES. Therefore, it will be called ICMULES (Implicit Corrected by MULES) in the following. The implicit step solves Eq. 9. In the present paper the following discretization schemes are used: implicit Euler in time, limited linear for the convective term with the relative flux, pure upwind for the other flux, a linear scheme for the gradient and linear with correction for the laplacian term.

The MULES algorithm is used in the next step to calculate an antidiffusive flux A, as previously, to ensure the boundedness of the solution. This antidiffusive flux is used to correct alpha similarly to Eq. 17:

$$\frac{\alpha^{corr}_{sp} - \alpha^i_{sp}}{\Delta t} V_p + \sum_f \lambda_f A = \alpha^{n+1}_{sp} S_i + S_e \qquad (18)$$

If the corrector step is used multiple times, an underrelaxation factor of 0.5 for all but the first iteration is introduced. It is usually applied three times in the following test cases.

Kinetic Theory Models

The solid phase fraction and its movement are modeled by the Kinetic Theory of Granular Flows (KTGF) (Gidaspow, 1994). A granular temperature Θ_s is used to model the solid phase viscosity and the particle pressure. Usually, a partial differential equation (PDE) for the granular temperature is constructed and solved (see (Gidaspow, 1994) or (Venier *et al.*, 2018) for further details).

If dissipation is assumed to be equal to production of the granular temperature, an algebraic equation is derived and solved instead of the PDE. (This is denoted in the OpenFOAM® settings by equilibrium=on).

For the solid viscosity $\mu_{s,ktgf}$ and the solid conductivity κ_s different models using the radial distribution function g_0, the granular temperature Θ_s and the restitution coefficient e_s exist.

Different models were proposed in literature for the calculation of the granular pressure, the frictional stress and the radial distribution function. A short recap of the used models is given below:

Granular Pressure Models

(a) Lun

$$p_s = \rho_s \alpha_s \Theta_s + 2\rho_s \alpha_s^2 g_0 \Theta_s \left(1 + e_s\right) \qquad (19)$$

For the granular pressure the relation presented by (Ding and Gidaspow, 1990) is used, which is derived based on Lun's velocity relations in a collision (Lun *et al.*, 1984).

Frictional Stress Models

The kinetic theory of granular flows does not model particle interactions with multiple neighboring particles near the packing limit, (Srivastava and Sundaresan, 2003; Venier *et al.*, 2018). Therefore, models to account for friction, frictional stress models, were introduced near the packing limit (when $\alpha_s > \alpha_{min}$). A frictional pressure and a frictional viscosity are added to the solid pressure and the solid viscosity:

$$p_s = p_{s,ktgf} + p_{s,fric} \qquad (20)$$

$$\mu_s = \mu_{s,ktgf} + \mu_{s,fric} \qquad (21)$$

Passalacqua and Fox (2011) and Venier *et al.* (2018) compare different frictional stress models and their influence on the simulation. Commonly used models are:

(a) Johnson Jackson (Johnson *et al.*, 1990)

$$p_{s,fric} = Fr \frac{\left(\alpha_s - \alpha_{min}\right)^\eta}{\left(\alpha_{s,max} - \alpha_s\right)^P} \qquad (22)$$

$$\mu_{s,fric} = 0.5 p_{s,fric} \sin(\phi) \qquad (23)$$

(b) Schaeffer (Schaeffer, 1987)

$$p_{s,fric} = 10^{25} \left(\alpha_s - \alpha_{s,min}\right)^{10} \qquad (24)$$

$$\mu_{s,fric} = 0.5 p_{s,fric} \left(I_{2D}\right)^{-1/2} \sin\left(\phi\right) \qquad (25)$$

The angle of internal friction Φ was set to 28 for the Schaeffer model and to 28.5 for the Johnson Jackson model in the simulations.

Radial Models

Different models to calculate the radial distribution function g_0 used in the granular pressure formulation (Eq. 19) have been proposed: (a) Carnahan Starling (Carnahan and Starling, 1969)

$$g_0 = \frac{1}{1-\alpha_s} + \frac{3\alpha_s}{2\left(1-\alpha_s\right)^2} + \frac{\alpha_s^2}{2\left(1-\alpha_s\right)^3} \tag{26}$$

(b) Lun Savage (Lun and Savage, 1986)

$$g_0 = \left(1 - \frac{\alpha_s}{\alpha_{max}}\right)^{-2.5\alpha_{max}} \tag{27}$$

(c) Sinclair Jackson (Lun and Savage, 1986; Sinclair and Jackson, 1989)

$$g_0 = \left(1 - \left(\frac{\alpha_s}{\alpha_{max}}\right)^{1/3}\right)^{-1} \tag{28}$$

It has to be noted, that the Carnahan Starling model does not take the maximum packing limit α_{max} into account, also emphasized by (Venier *et al.*, 2016). Therefore, the choice of the frictional stress model in conjunction with this model is essential, which will also be shown in the Results section.

RESULTS

Common test cases for two-fluid models are chosen to test the stability of the newly proposed algorithm. The results are compared to simulations with MULES. Furthermore, the influence of different frictional stress and radial models was tested to ensure the applicability of the ICMULES with different settings.

The test cases and the corresponding models used are summarized in Table 1. The abbreviations there correspond to the test cases: falling block=f.b., settling suspension=s.s., bubble growth=b.g. and raceway=r.w.. The letters (a)/(b)/(c) correspond to the models described in the section about the kinetic theory.

In the following subsections the chosen test cases are described and their results are presented.

Table 1: Models for the kinetic theory used for the different test cases and the chosen parameters

Model	f.b.	s.s.	b.g.	r.w.
equilibrium	off	off	off	off
viscosity	(a)	(b)	(b)	(b)
conductivity	(a)	(b)	(b)	(b)
granular pressure	(a)	(a)	(a)	(a)
frictional stress	(a)	(a)/(b)	(b)	(b)
radial	(a)	(c)	(a)/(b)	(c)
Parameters				
packing limit	0.63	0.60	0.63	0.63
α_{min}	0.60	0.55	varying	0.6
restitution coeff.	0.80	0.80	0.95	0.95

Falling Block (f.b.)

The falling block test case is chosen to check the stability of the algorithm. It was also used by (Passalacqua and Fox, 2011) and (Venier *et al.*, 2013). A block (dimensions: 0.026 m x 0.08 m) with a solid volume fraction of 0.58 is introduced at a height of 0.012 m in a 2D-domain with 0.05 m width and 0.2 m height. It falls down solely by gravity. A hexahedral mesh with 10 x 40 cells is used for the simulation in OpenFOAM® .

The particles have a diameter of 0.4 mm and a density of 2000 kg/m^3. The fluid phase viscosity is $1.84{\cdot}10^{-5}$ Pa·s and a Prandtl Number of 0.7 is used. No virtual mass effects are taken into account and the drag is modeled as suggested by (Gidaspow, 1994), blending the Ergun and the Wen-Yu drag models.

The velocity boundary conditions are set as Dirichlet boundary conditions at the bottom and top for particle velocity and at the walls and the bottom for the air velocity. A Neumann boundary condition is set for the air velocity at the top and the particle velocity at the walls.

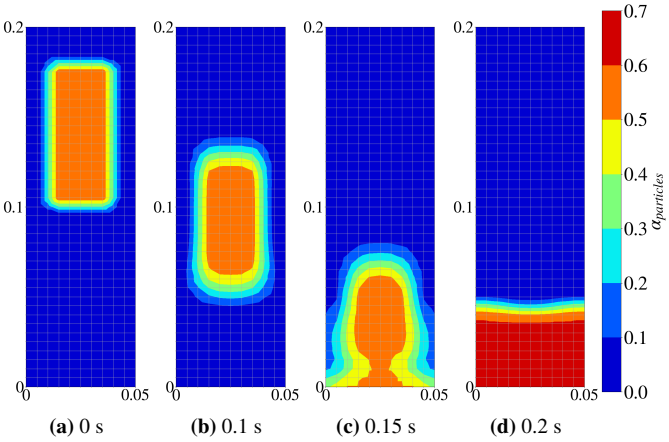

(a) 0 s **(b)** 0.1 s **(c)** 0.15 s **(d)** 0.2 s

Figure 1: Falling block using MULES algorithm

The results using MULES and ICMULES are shown in Figure 1 and Figure 2, respectively. The results are very similar for the both algorithms. The particles are slightly denser packed when using the ICMULES algorithm. The snapshot at 0.2 s is not the finally settled bed.

The difference in the maximum packing could be related to the chosen radial and frictional stress model. The used radial model (Carnahan Starling) does not take the maximum packing limit into account. It is also discussed by (Schneiderbauer *et al.*, 2012), that the maximum packing limit is ensured by the divergence of the frictional stresses, when the Carnahan Starling or a similar model is used for the radial distribution function. The MULES algorithm is still enforcing the packing limit by accounting for it in the flux reconstruction. The correction step in the ICMULES is not enforcing this limit. The question remains if this property is related to a physical model or it is a "numerical" trick in the MULES algorithm. Probably, one should anyways aim to choose a physically valid combination of radial model and frictional stress model, which ensures the packing limit.

Settling Suspension (s.s.)

The settling supension case uses also a 2D-setup with 0.05 m width and 0.3 m height and is discretized by 8 x 40 hexahedral cells. The whole column is initialized with a solid volume fraction of 0.3. Through gravity, the particles settle after time until they reach the packing limit ($\alpha_{max} = 0.6$). Passalacqua and Fox (2011) use this case to test an implicit solution. Venier *et al.* (2016) use it to compare partial elimination with partially implicit approach for the decoupling of the momentum equations.

The properties of the solid and fluid fraction are the same as for the falling block case, except that the Prandtl number was

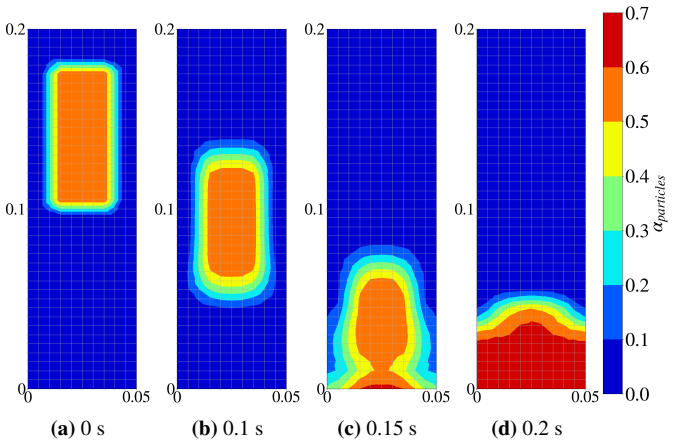

Figure 2: Falling block using ICMULES

set to unity for both phases. The boundary conditions as well as the virtual mass and drag effects are treated in the same way as for the falling block case.

The solid void fraction profiles after different settling times are shown in Figure 3. The two algorithms are compared to the literature data from (Passalacqua and Fox, 2011) and (Venier *et al.*, 2016). Here, two different frictional stress models, the Johnson and Jackson (a) and the Schaeffer (b) model were applied.

Figure 3 shows, that the MULES and ICMULES case agree very well at the later settling times. In the beginning, at t = 0.1 s, there is a difference at the top of the column. We are not entirely sure, what is causing those differences between the MULES and ICMULES results. Because the ICMULES algorithm fits better to the presented literature data the presented algorithm seems valid. One reason for the differences at the beginning and the top of the column could be that numerical diffusion is more pronounced when applying the MULES algorithm.

At later times, the major difference between the solutions results from the different frictional stress models. The Schaeffer (b) model limits the phase fraction already to the α_{min} value. The results from the JohnsonJackson (a) model agree well with the results from literature and the results from ICMULES and MULES are virtually identical for the later time steps (t = 0.6 seconds).

Bubble Growth (b.g.)

The 2D bubble growth case checks the bubble growth in a fluidised bed with a central jet. Venier *et al.* (2018) studied the influence of the third dimension and did not find a significant impact, therefore, we only use the 2D case here. The geometry is 0.57 m wide and 1 m high and is discretized by 112 x 200 cells, which was determined to be the "best" mesh regarding the trade-off between calculation time and accuracy (Venier *et al.*, 2018).

First, the bubble formation with no frictional stress - or more precisely $\alpha_{min} > \alpha_{max}$ to avoid the contribution of frictional stresses was studied, see previous section about the frictional stress models. This was done to eliminate the influence of the chosen frictional stress model on the test results and solely study the influence of the radial model.

When using the ICMULES algorithm, the choice of the radial model determines if the packing limit is ensured, as discussed in the previous section. The ICMULES can enforce the packing limit when using the radial distribution models of Lun

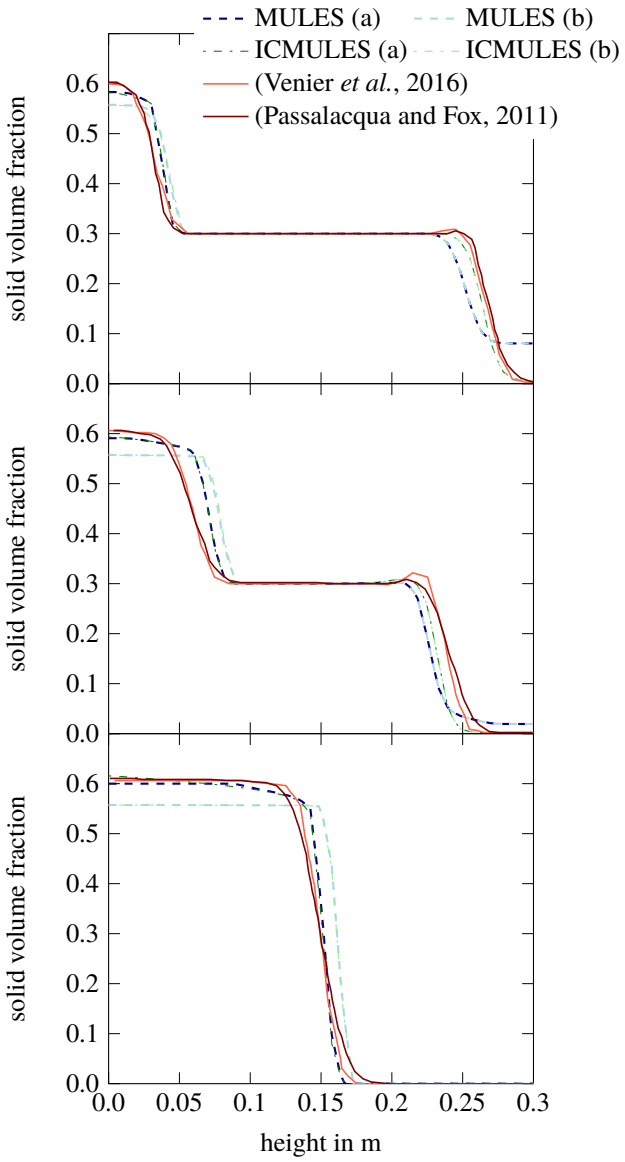

Figure 3: Solid volume fraction α_s after t = 0.1, 0.15 and 0.6 seconds settling time (from top to bottom), (a) and (b) refer to the frictional stress model

Savage or Sinclair Jackson, because there α_{max} is used in the formulations. The contribution of the radial function g_0 has a singularity at the packing limit and avoids overpacking in that way. When the Carnahan Starling model is used, the ICMULES cannot enforce the packing limit, see Figure 4 (d). The results in Figure 4 (d) show clearly, that the ICMULES is not applicable without a proper frictional stress model near the packing limit.
The MULES algorithm can always enforce the packing limit, because α_{max} is given as an input parameter for the flux calculation and ensures α values between 0 and α_{max} through the algorithmic implementation.
When the results without frictional stress with the Lun Savage radial model are compared, they are identical for the explicit and implicit algorithm, see Figure 4. The agreement with the experiments seems though to be best for the Carnahan Starling model using the explicit algorithm. Comparing the simulated and measured bubble detachment time, Table 2 indicates that the Lun Savage model agrees better with the experiments.

Table 2: Bubble detachement time in seconds. Experimental values from (Kuipers *et al.*, 1991). Simulations without frictional stress model

Exp.	MULES		ICMULES		
	(a)	(b)	(a)	(b)	radial model
0.17	0.19	0.15	0.31	0.15	

The simulations without frictional stress model were conducted to highlight the differences of the algorithmic approaches. For simulations near the packing limit it is usually not advised to ignore the frictional stresses, because the kinetic theory can not account for multiple particle interactions. Therefore, we also studied the bubble formation with a frictional stress model. We chose the Schaeffer frictional stress model, because it can be applied with the Carnahan Starling radial model. The results of the bubble formation at t = 0.1, 0.14 and 0.18 s are also shown in Figure 4. The minimum frictional packing was set to $\alpha_{min} = 0.6$.
Kuipers *et al.* (1991) presented also the bubble diameter ratio of the experiments. Figure 5 compares those ratios with the ones from the simulation without frictional stress. In the simulation the bubble was measured as the region with a void fraction below 0.2. The bubble shape with the Lun Savage radial model and no frictional stresses is predicted in line with the experiments for the first 0.15 seconds. Then, the vertical stretch is over and/or the longitudinal stretch under predicted. The same comparison was made for the bubble prediction using the Schaeffer frictional stress model, see Figure 6. Here the longitudinal stretch of the bubble seems way overpredicted. This is already visible in Figure 4. Nevertheless, the bubble diameter ratio shows, that the algorithm is not influencing the results. The deviations between simulation and experiments are most likely related to the models and settings chosen therein.

2D Raceway (r.w.)

The last studied test case in this paper is a 2D Raceway formation test case. The test case was first presented by (Feng *et al.*, 2003). They studied the raceway formation in a simple 2D-setup by DEM simulation. Here, we test the applicability of an Euler-Euler algorithm in the prediction of the raceway formation in comparison with those DEM results. Furthermore, we test the proposed algorithm ICMULES and study the simulation time in comparison with the original algorithm.

Experiments from (Kuipers *et al.*, 1991)

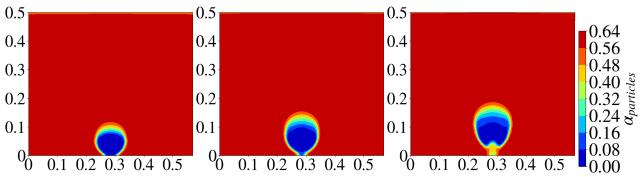

(a) MULES algorithm without frictional stress, Lun Savage model

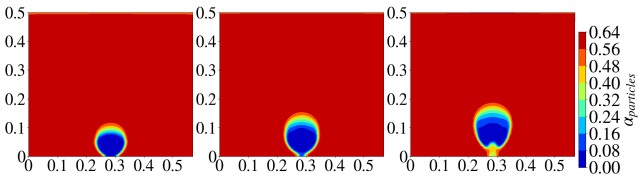

(b) ICMULES algorithm without frictional stress, Lun Savage model

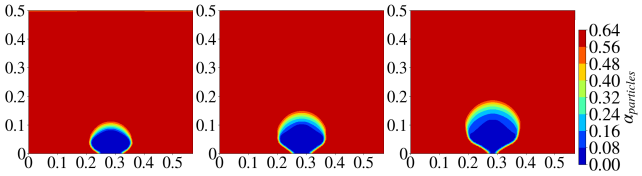

(c) MULES algorithm without frictional stress, Carnahan Starling model

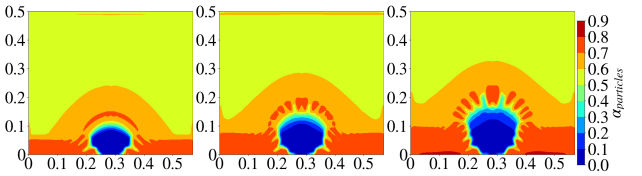

(d) ICMULES algorithm without frictional stress, Carnahan Starling model

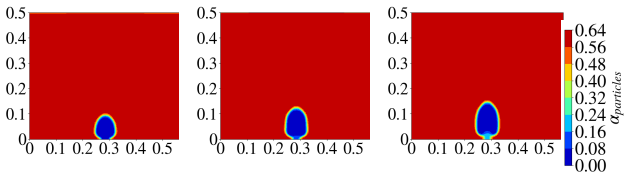

(e) MULES algorithm with Schaeffer frictional stress model, Carnahan Starling model

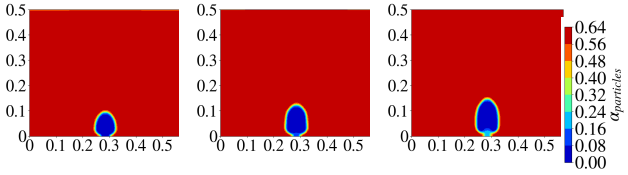

(f) ICMULES algorithm with Schaeffer frictional Stress model, Carnahan Starling model

Figure 4: Single Bubble after 0.1, 0.14 and 0.18 seconds (column-wise).

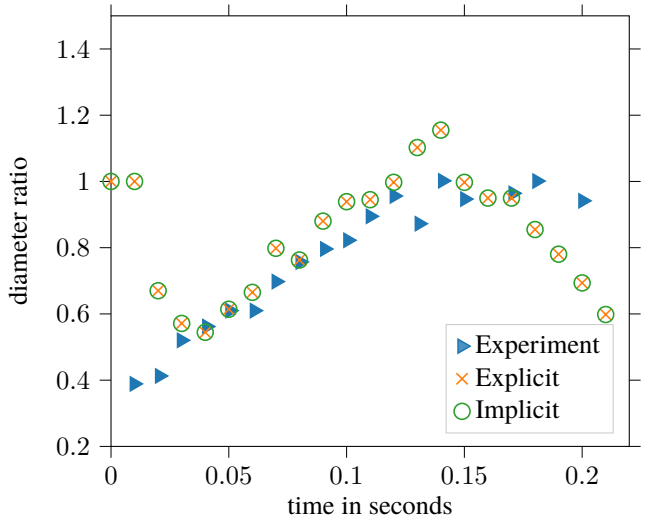

Figure 5: Comparison of the diameter ratio for the experiments from (Kuipers *et al.*, 1991) and the simulations using No Frictional Stress and Lun Savage radial model

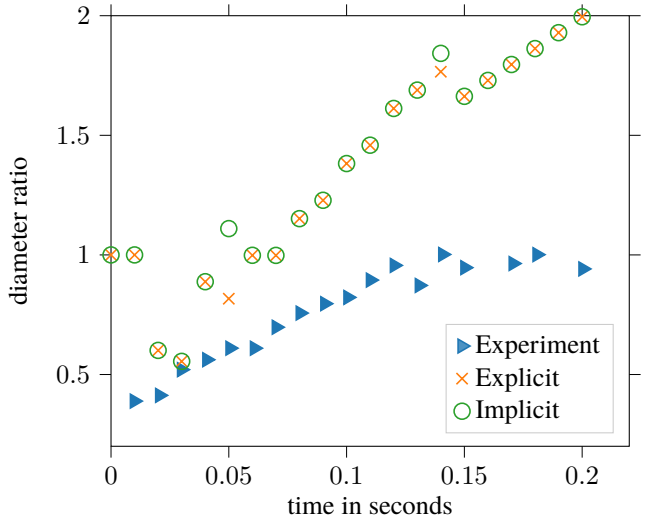

Figure 6: Comparison of the diameter ratio for the experiments from (Kuipers *et al.*, 1991) and the simulations using Schaeffer and Carnahan Starling model

The raceway is simulated as a 2D raceway, same as by (Feng *et al.*, 2003). The bed is 1 m high and 0.3 m wide. It was discretized by a uniform mesh using 200x60 cells. The jet inlet is positioned 0.1 m above the bottom of the bed and is 0.02 m wide. Table 3 lists the physical parameters for solid and gas phase used in the simulation.

Neumann boundary conditions for the air velocity are set at the walls and bottom. The inlet velocity is set to 20, 25 and 30 m/s for the different cases studied. At the top, the air pressure is fixed and no inflow is allowed. The particle velocity is set to zero at the inlet and outlet and a partial slip condition is used at the wall and bottom (Johnson and Jackson, 1987) with a specularity coefficient of one. The specularity coefficient defines the degree of frictional interaction between walls and particles (specularity coefficient = 0 corresponds to frictionless walls). The velocity at the boundary is calculated based on this interaction coefficient. The granular temperature at the walls and bottom is also treated by the JohnsonJackson-

Table 3: simulation parameters for the raceway case

Solid phase		
diameter	m	0.004
density	kg/m^3	2500
Gas phase		
density	kg/m^3	1.205
viscosity	kg/(ms)	$1.8{\cdot}10^{-5}$

ParticleTheta conditions, described in (Johnson and Jackson, 1987), using the same specularity coefficient and a restitution coefficient of 0.95.

As a result of the previous test cases, we decided to use the Schaeffer frictional stress model and the Carnahan Starling radial model for the simulations. The maximum packing limit was set to $\alpha_{max} = 0.63$ and the minimum frictional velocity to $\alpha_{min} = 0.6$.

Figure 7 and Figure 8 show the results from the raceway formation for two different inlet velocities: 25 and 30 m/s. For the 20 m/s practically no raceway is formed, which qualitatively agrees with the presented results in (Feng *et al.*, 2003). For the case with 25 m/s inlet velocity, the raceway is reaching a steady state after some time. For 30 m/s inlet velocity the bed performs more like a bubbly bed and the raceway does not seem to reach a steady state. The MULES and ICMULES algorithms give the same results for the raceway formation. For these cases a fixed time step of 10^{-5} s was used.

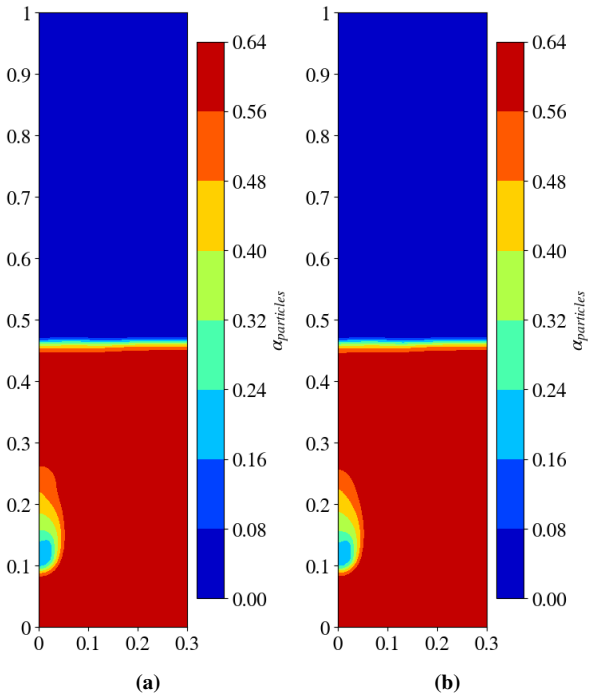

Figure 7: Raceway formation for 25 m/s inlet velocity after 1 s simulation time for the different algorithms: (a) MULES (b) ICMULES

We also compare the raceway penetration depths from (Feng *et al.*, 2003) and the simulations. It is not entirely clear, how the raceway penetration depth is defined by Feng *et al.* (2003). Here it was calculated as the distance from the air inlet to the region with a void fraction above 0.3. Table 4 shows the results from the simulation and literature. The penetration depth agrees well for the cases of high velocity (30 and 25 m/s). For 20 m/s no raceway is formed in the

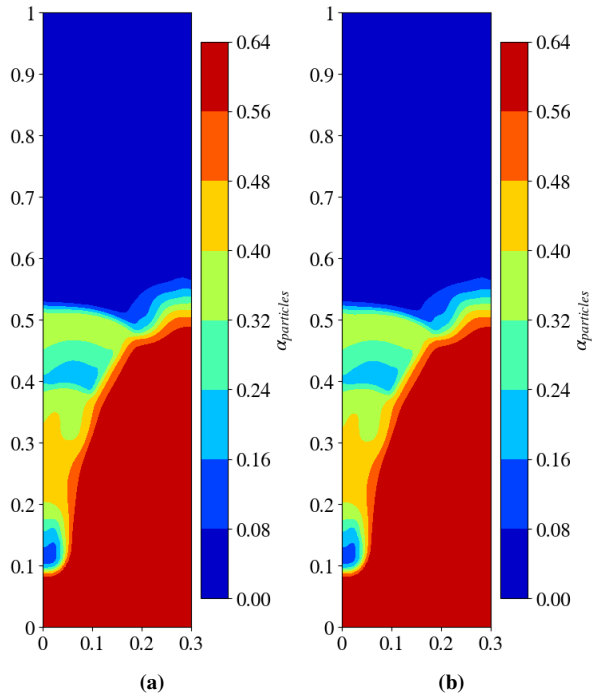

Figure 8: Raceway formation for 30 m/s inlet velocity after 1 s simulation time for the different algorithms: (a) MULES (b) ICMULES

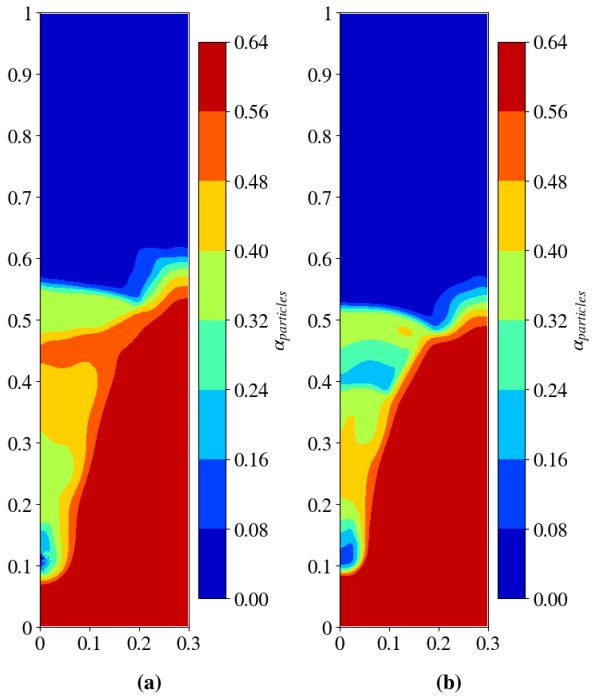

Figure 9: Raceway formation for 30 m/s inlet velocity after 1 s simulation time for the different algorithms using variable time stepping with maxCo = 0.6: (a) MULES (b) ICMULES

OpenFOAM® simulations. Better agreement might be obtained, by also accounting for virtual mass effects, which were neglected here.

Table 4: Raceway penetration depth in mm in comparison

	paper	explicit	implicit
0.30 m/s	42	41	41
0.25 m/s	30	32	32
0.20 m/s	25	-	-

The above test cases were all tested with the same time step sizes for MULES and ICMULES and consequently resulted in approximately the same computational time. To give an indication on the possible computational improvements through the ICMULES, we also tested the Raceway case with variable time step using a maximum Courant number of 0.6. The computational time of the two cases yields 13805 s using MULES and 4008 s using ICMULES.
Figure 9 shows the results of the simulations with bigger time steps. This reveals, that the results from MULES with a bigger time step are not consistent with the results with lower time step. Contrary, the results from ICMULES agree well with the results in Figure 8.

CONCLUSION

In nearly all the test cases the newly introduced algorithm ICMULES gave similar results as the MULES algorithm. Only for certain model combinations, where the packing limit is not ensured through the radial or frictional stress model, the results differ significantly. There, the ICMULES algorithm fails to enforce the packing limit. This might be a limitation of the newly proposed algorithm. On the contrary, the question remains, if the packing limit should be enforced purely by numerical treatment, if the frictional or the radial model does not depict this packing limitation.

First results were presented, showing that the ICMULES enables considerable speed-up, since it produces consistent results also for higher Courant numbers, i.e. time steps.
In conclusion, the introduced algorithm can be used for the simulation of gas-solid systems, also near the packing limit, if suitable frictional and radial models are chosen.

ACKNOWLEDGMENT

The authors gratefully acknowledge the funding support of K1-MET GmbH, metallurgical competence center. The research program of the competence center K1-MET is supported by COMET (Competence Center for Excellent Technologies), the Austrian program for competence centers. COMET is funded by the Federal Ministry for Transport, Innovation and Technology, the Federal Ministry for Digital and Economic Affairs, the province of Upper Austria, Tyrol, and Styria. Apart from funding, the project activities are financed by the industrial partners Primetals Technologies Austria, voestalpine Stahl and voestalpine Stahl Donawitz.

REFERENCES

ABHALE, P.B., VISWANATHAN, N.N. and SAXEN, H. (2020). “Numerical Modelling of blast furnace – Evolution and recent trends”. *Mineral processing and Extractive Metallurgy*, **129(2)**, 166–183.

AGRAWAL, K., LOEZOS, P.N., SYAMLAL, M. and SUNDARESAN, S. (2001). “The role of meso–scale structures in rapid gas–solid flows”. *J. Fluid Mech.*, **445**, 151–185.

CARNAHAN, N.F. and STARLING, K.E. (1969). “Equation of state for nonattracting rigid spheres”. *The Journal of Chemical Physics*, **51(2)**, 635–636.

DING, J. and GIDASPOW, D. (1990). “A bubbling fluidization model using kinetic theory of granular flow”. *AIChE Journal*, **36(4)**, 523–538.

FENG, Y.Q., PINSON, D., YU, A.B. and ZULLI, P. (2003). "Numerical Study of Gas-Solid Flow in the Raceway of a Blast Furnace". *Steel research*, **74(9)**, 523–530.

GIDASPOW, D. (1994). *Multiphase Flow and Fluidization - Continuum and Kinetic Theory Descriptions*. Academic Press, Inc.

JOHNSON, P. and JACKSON, R. (1987). "Frictional-collisional constitutive relations for granular materials, with application to plane shearing". *J. Fluid Mech.*, **179**, 67–93.

JOHNSON, P., NOTT, P. and JACKSON, R. (1990). "Frictional–Collisional Equations of Motion for Granular Materials and Their Application to chutes". *Journal of Fluid Mechanics*, **210**, 501–535.

KUIPERS, J., PRINS, W. and VAN SWAAIJ, W. (1991). "Theoretical and Experimental Bubble Formation at a Single Orifice in a Two-Dimensional Gas-Fluidized Bed". *Chemical Engineering Science*, **46(11)**, 2881–2894.

LUN, C.K. and SAVAGE, S.B. (1986). "The effects of an impact velocity dependent coefficient of restitution on stresses developed by sheared granular materials". *Acta Mechanica*, **63(1-4)**, 15–44.

LUN, C.K., SAVAGE, S.B., JEFFREY, D.J. and CHEPURNIY, N. (1984). "Kinetic theories for granular flow: Inelastic particles in Couette flow and slightly inelastic particles in a general flowfield". *Journal of Fluid Mechanics*, **140**, 223–256.

OLIVEIRA, P.J. and ISSA, R.I. (2003). "Numerical aspects of an algorithm for the Eulerian simulation of two-phase flows". *International Journal for Numerical Methods in Fluids*, **43(10-11)**, 1177–1198.

PAPADIKIS, K., BRIDGWATER, A. and GU, S. (2008). "CFD modelling of the fast pyrolysis of biomass in fluidised bed reactors, Part A: Eulerian computation of momentum transport in bubbling fluidised beds". *Chemical Engineering Science*, **63**, 4218–4227.

PASSALACQUA, A. and FOX, R.O. (2011). "Implementation of an iterative solution procedure for multi- fluid gas–particle flow models on unstructured grids". *Powder Technology*, **213**, 174–187.

RUSCHE, H. (2002). *Computational Fluid Dynamics of Dispersed Two-Phase Flows at High Phase Fractions*. Ph.D. thesis, Imperial College of Science, Technology & Medicine.

SCHAEFFER, D.G. (1987). "Instability in the evolution equations describing incompressible granular flow". *Journal of Differential Equations*, **66(1)**, 19–50.

SCHNEIDERBAUER, S., AIGNER, A. and PIRKER, S. (2012). "A comprehensive frictional-kinetic model for gas-particle flows: Analysis of fluidized and moving bed regimes". *Chemical Engineering Science*, 279–292.

SINCLAIR, J.L. and JACKSON, R. (1989). "Gas particle flow in a vertical pipe with particle particle interactions". *AIChE Journal*, **35(9)**, 1473–1486.

SRIVASTAVA, A. and SUNDARESAN, S. (2003). "Analysis of a frictional-kinetic model for gas-particle flow". *Powder Technology*, **129**, 72–85.

TACCONI, Z. (2018). *Feasibility analysis of a two-fluid solver for cavitation and interface capturing as implemented in OpenFOAM*. Tesi di laurea, Politecnico Di Milano.

VAN DER HOEF, M., VAN SINT ANNALAND, M., DEEN, N. and KUIPERS, J. (2008). "Numerical Simulation of Dense Gas–Solid Fluidized Beds: A Multiscale Modeling Strategy". *Annu. Rev. Fluid Mech.*, **40**, 47–70.

VENIER, C., DAMIAN, S.M., RAMAJO, D. and NIGRO, N. (2013). "Numerical analysis of Multiphase Solid-Gas Flow with Eulerian Models and Kinetic Theory Closure". *Mecánica Computacional*, **XXXII**, 1849–1862.

VENIER, C.M., MARQUEZ, S. and NIGRO, N.M. (2016). "Numerical aspects of Eulerian gas – particles flow formulations". *Computers and Fluids*, **133**, 151–169.

VENIER, C.M., Marquez Damian, S. and NIGRO, N.M. (2018). "Assessment of gas–particle flow models for pseudo-2D fluidized bed applications". *Chemical Engineering Communications*, **205(4)**, 456–478.

WARDLE, K.E. and WELLER, H.G. (2013). "Hybrid Multiphase CFD Solver for Coupled Dispersed/Segregated Flows in Liquid-Liquid Extraction". *International Journal of Chemical Engineering*, 1–13.

WELLER, H. (2005). "Derivation, Modelling and Solution of the Conditionally Averaged Two-Phase Flow Equations". Tech. rep.